Published in final edited form as:

Nature. 2019 October ; 574(7777): 264–267. doi:10.1038/s41586-019-1608-2.

The Fungal Mycobiome Promotes Pancreatic Oncogenesis via MBL Activation

Berk Aykut[*,1], **Smruti Pushalkar**[*,2], **Ruonan Chen**[1], **Qianhao Li**[2], **Raquel Abengozar**[1], **Jacqueline I. Kim**[1], **Sorin A. Shadaloey**[1], **Dongling Wu**[1], **Pamela Preiss**[1], **Narendra Verma**[3], **Yuqi Guo**[2], **Anjana Saxena**[4], **Mridula Vardhan**[2], **Brian Diskin**[1], **Wei Wang**[1], **Joshua Leinwand**[1], **Emma Kurz**[1], **Juan A. Kochen Rossi**[1], **Mautin Hundeyin**[1], **Constantinos Zambrinis**[1], **Xin Li**[2], **Deepak Saxena**[#,1,2], **George Miller**[#,1,5]

[1]S. Arthur Localio Laboratory, Department of Surgery, New York University School of Medicine, 550 First Avenue, New York, NY 10016

[2]Department of Basic Science and Craniofacial Biology, New York University College of Dentistry, 345 E. 24th Street, New York, NY 10010

[3]Department of Medicine, New York University School of Medicine, 550 First Avenue, New York, NY 10016

Address correspondence to: George Miller, MD, Departments of Surgery and Cell Biology, New York University School of Medicine, 435 East 30th Street, Room 417, New York, NY 10016, Tel: (646) 501-2208, Fax: (212) 263-6840, george.miller@nyumc.org, Deepak Saxena, Ph.D, Department of Basic Science and Craniofacial Biology, New York University College of Dentistry, 345 E. 24th Street, Room 921B, New York, NY 10010, Tel.: (212) 998-9256, ds100@nyu.edu. **Correspondence and requests for materials** should be addressed to G.M. or D.S.

[*]Contributed equally

[#]Co-senior authors

Author Contributions

B.A. (berk.aykut@nyulangone.org) carried out *in vivo* and *in vitro* experiments, study design, PCR, analysis and interpretation, manuscript preparation, and statistical analysis; S.P. (sp117@nyu.edu) carried out fungal DNA sequencing, analysis and interpretation, manuscript preparation, and statistical analysis; R.C. (rc3266@nyu.edu) carried out *in vivo* experiments, histological analysis, and manuscript preparation; Q.L. (ql770@nyu.edu) performed computational analyses and provided critical review; R.A. (raquelabengozar@yahoo.es) carried out *in vivo* experiments and provided technical assistance; J.I.K. (jacqueline.kim@nyulangone.org) carried out *in vivo* experiments and provided critical review; S.A.S. (sorinarmanalberto.shadaloey@nyulangone.org) carried out mouse breeding and histology; D.W. (emmawudongling@gmail.com) performed tissue culture and cell line generation; P.P. (pamela_preiss@gmx.de) provided technical assistance and carried out *in vivo* experiments; N.V. (narendra.verma@nyulangone.org) carried out knockdown experiments; Y.G. (yg701@nyu.edu) carried out PCR; A.S. (asaxena@brooklyn.cuny.edu) performed FISH and provided critical review; M.V. (mridula.vardhan@gmail.com) carried out DNA extraction and contributed to computational analysis; B.D. (brian.diskin@nyulangone.org) carried out *in vivo* experiments and critical review; W.W. (wei.wang3@nyulangone.org) provided technical assistance; J.L. (joshua.leinwand@nyulangone.org) provided critical review and contributed to study design; E.K. (emma.kurz@nyulangone.org) carried out *in vivo* experiments and contributed to study design; J.A.K.R. (juan.kochenrossi@nyulangone.org) provided technical assistance and contributed to study design; M.H. (mautinhundeyin@gmail.com) carried out *in vivo* experiments; C.Z. (zambri@gmail.com) carried out human sample collection; X.L. (xl15@nyu.edu) provided technical assistance; D.S. (ds100@nyu.edu) and G.M. (george.miller@nyulangone.org) conceived, designed, supervised, analyzed, and interpreted the study, prepared the manuscript, and provided critical review.

Competing interests

The authors declare no competing interests.

Figure Preparation

Figures were prepared with BioRender software and Indesign (Adobe).

Data Availability

Sequence data sets analyzed in this article are publicly available in the NCBI BioProject database under the accession number PRJNA557226. Raw data for all experiments are available as Source Data to the relevant figures.

[4]Biology Department, Brooklyn College NY 11210 and Biology/Biochemistry Programs, Graduate Center (CUNY), New York, NY 10016

[5]Department of Cell Biology New York University School of Medicine, 550 First Avenue, New York, NY 10016

Abstract

Bacterial dysbiosis has emerged as an accomplice to carcinogenesis in malignancies such as colon and liver cancer, and we have recently implicated the microbiome in the pathogenesis of pancreatic ductal adenocarcinoma (PDA)[1]. However, the mycobiome has not been clearly implicated in tumorigenesis. We found that fungi migrate from the gut lumen to the pancreas. PDA tumors harbored a ~3000-fold increase in fungi compared to normal pancreas in both mice and humans. The composition of the PDA mycobiome was distinct from that of gut or normal pancreas based on alpha and beta diversity indices. Specifically, the fungal community infiltrating PDA tumors was markedly enriched for *Malassezia* in both mice and humans. Fungal ablation was tumor-protective in slowly progressive and invasive models of PDA whereas repopulation with *Malassezia* – but not *Candida*, *Saccharomyces*, or *Aspergillus* – accelerated oncogenesis. In parallel, we discovered that ligation of mannose-binding lectin (MBL), which binds fungal wall glycans to activate the complement cascade, was required for oncogenic progression whereas MBL or C3 deletion in the extra-tumoral compartment or C3aR knockdown in tumor cells were protective. Further, reprogramming of the mycobiome did not alter PDA progression in *Mbl* or *C3* deficient mice. Collectively, our work shows that pathogenic fungi promote PDA by driving the complement cascade via MBL activation.

Keywords

Pancreatic cancer; fungi; MBL; complement

We recently reported that intra-pancreatic bacteria expand ~1000-fold in PDA[1]. Similarly, we discovered a marked increase in the intra-tumoral fungi in human PDA and in mouse models (Fig. 1a–d). Since there is direct communication between the gut and pancreatic duct via the sphincter of Oddi, we postulated that endoluminal fungi can access the pancreas. To test this, we administered GFP-labeled *Saccharomyces cerevisiae* to control or tumor-bearing mice via oral gavage. Fungi migrated into the pancreas within 30 minutes, suggesting that the gut mycobiome can directly influence the pancreatic microenvironment (Fig. 1e).

We next assessed for evidence of fungal dysbiosis during tumorigenesis using $p48^{Cre}$;$LSL\text{-}Kras^{G12D}$ (KC) mice, which express oncogenic *Kras* in their pancreatic progenitor cells and develop slowly progressive PDA[2]. Comparison of the gut and intra-pancreatic fungal communities in 30-week old KC mice by Principal Coordinate Analysis (PCoA) suggested that the gut and tumor mycobiomes clustered separately (Fig. 1f). Further, we observed reduced alpha diversity in the transformed pancreas compared to the gut (Fig. 1g). *Ascomycota* and *Basidiomycota* were the only phyla detected in pancreatic tissue, whereas *Mortierellomycota* and *Mucoromycota* were additionally detected in the gut at low

abundance (Fig. 1h). The most prevalent genus in the KC pancreata was *Malassezia* at ~20% abundance, which was markedly increased in relative abundance compared to gut (Fig. 1i). Of note, benign pancreatic inflammation did not increase fungal infiltration in the pancreas (Extended-Data Fig. 1).

To determine whether the gut mycobiome is reprogrammed during the course of oncogenesis, we performed a longitudinal analysis of fecal samples from KC mice and littermate controls. PCoA analysis suggested that whereas WT and KC mice had similar fungal communities early in life, by 30 weeks differences in beta-diversity were noted in the gut of KC mice compared to WT (Fig. 1j–l). Accordingly, fungal communities in the gut of KC and WT mice differed considerably at 30 weeks (Extended-Data Fig. Fig. 2).

We next analyzed the fecal and tumor mycobiome in PDA patients. Similar to mice, *Ascomycota* and *Basidiomycota* were the most common phyla in the gut and in tumor tissue (Fig. 2a). At the genus level, parallel to our mice data, *Malassezia* was more prevalent in tumor tissues compared to gut (Fig. 2b). Moreover, alpha-diversity analyses revealed significant differences between human PDA tumor tissue and gut (Fig. 2c). PCoA confirmed distinct clustering of fungal communities in the tumor tissue and gut of PDA patients (Fig. 2d). Further, the mycobiome in human PDA clustered separately from that of normal human pancreas (Fig. 2e). Collectively, these data indicate that human PDA tumors harbor a mycobiome that is distinct from gut or normal pancreas.

To determine the influence of fungal dysbiosis on PDA progression, we ablated the mycobiome using oral Amphotericin B in the KC model. Fungal ablation protected against oncogenic progression (Fig. 3a). Similarly, Amphotericin B was protective in an aggressive orthotopic PDA model using tumor cells derived from $Pdx1^{Cre};Kras^{G12D};Tp53^{R172H}$ (KPC) mice (Fig. 3b)[3]. Fungal ablation potentiated the effect of Gemcitabine-based chemotherapy (Fig. 3c). Of note, treatment with fluconazole was also protective (Extended-Data Fig. 3a). However, anti-fungals did not offer tumor-protection in germ-free mice (Extended-Data Fig. 3b). Further, consistent with absence of increased fungal infiltration in pancreatitis, anti-fungals did not ameliorate benign pancreatic inflammation (Extended-Data Fig. 3c–e).

To confirm that fungal dysbiosis accelerates PDA, we repopulated Amphotericin B-treated mice with *Malassezia globosa*, which is at increased abundance in mouse and human PDA (Figs. 1i and 2b). Of note, the *M. globosa* ATCC strain used in repopulation experiments had 100% sequence identity to the *Malassezia* taxon that was the most abundant in PDA (Supplemental Table 1). Controls were repopulated with *Candida sp.*, *S. cerevisae*, or *Aspergillus sp.* or treated with vehicle. Only *M. globosa* accelerated PDA growth whereas the other taxa had no effect (Fig. 3d). Repopulation with *C. tropicalis* also did not accelerate PDA growth (Extended-Data Fig. 3f).

MBL is a mannose binding lectin that recognizes fungal pathogens and activates the lectin pathway of the complement cascade[4]. *MBL* expression was associated with reduced survival in human PDA based on TCGA transcriptomic data (Extended-Data Fig. 4a). We postulated that fungi may promote tumorigenesis via MBL activation. Accordingly, KC;MBL-null mice exhibited delayed oncogenic progression (Fig. 4a). *Mbl* deletion was also protective against

orthotopic KPC tumor growth and resulted in extended animal survival (Fig. 4b, c). Moreover, Amphotericin B treatment did not provide tumor-protection in MBL-null mice (Extended-Data Fig. 4b). Similarly, *Malassezia*, which binds C-type lectin receptors[5], failed to accelerate tumor progression in MBL-null mice (Extended-Data Fig. 4c).

The C3 complement cascade has been investigated in PDA and other cancers and is potently oncogenic via diverse mechanisms including increasing tumor cell proliferation, motility, and invasiveness, and corrupting adaptive immune responses[6,7]. Since MBL initiates the lectin pathway of the complement cascade triggering C3 convertase, we postulated that the Fungal-MBL axis promotes PDA progression via complement activation. Similar to *MBL*, *C3* expression was associated with a trend toward reduced survival in human PDA (Extended-Data Fig. 4d). We found robust expression of C3a in pancreata of KC mice, and this was nearly absent in WT or KC;MBL-null mice (Extended-Data Fig. 4e). Consistent with our hypothesis, recombinant C3a accelerated KPC cellular proliferation *in vitro* (Extended-Data Fig. 4f) and tumor growth *in vivo* (Fig. 4d) while *C3*-deficient mice were protected against PDA (Fig. 4e). Similarly, C3aR knockdown in PDA cells (Fig. 4f) mitigated tumor growth (Fig. 4g). Moreover, we found that targeting the mycobiome had no additional efficacy in C3-deficient animals (Fig. 4h). In aggregate, these data indicate that the pancreatic mycobiome requires the MBL-C3 axis to promote tumor growth.

In summary, we found that fungi migrate from the gut to the pancreas, and PDA tumors harbor a marked expansion in the pancreatic mycobiome. The composition of the PDA mycobiome was distinct from that of gut or normal pancreas and was enriched for *Malassezia* in both mice and humans. Mycobial ablation was protective against PDA, whereas repopulation with *Malassezia* – but not other commensal fungi – accelerated oncogenesis. Whether mycobial reprogramming is a cause or consequence of oncogenesis is difficult to answer fully. However, our fungal adoptive transfer and fungal ablation experiments suggest that select fungi are sufficient to promote PDA progression. It is likely that, akin to observations regarding the microbiome[1], oncogeneic *Kras*-induced inflammation leads to the fungal dysbiosis which in-turn promotes tumor progression via activation of the MBL-C3 cascade (Fig. 4i). Of note, as the mycobiome influences the microbiome and vice-versa[8], more exact study is required to assess this dynamic crosstalk in PDA. Collectively, our work suggests that the mycobiome may be a new target for therapeutics and area for biomarker discovery.

Methods

Animals and tumor models

KC mice, which develop spontaneous pancreatic neoplasia by targeted expression of mutant *Kras* in the pancreas, were a gift from Dafna Bar-Sagi (New York University)[2]. C57BL/6, MBL-null, and $C3^{-/-}$ mice were originally purchased from Jackson Labs (Bar Harbor, ME) and were bred in-house. Littermates were used as controls. Animals were housed under specific pathogen-free conditions and fed standard mouse chow. In select experiments, C57BL/6 mice generated and housed in a germ-free facility were utilized. Longitudinal cohort studies were conducted to monitor microbial communities throughout experiments by serially collecting fecal specimens from littermate WT and KC mice. For orthotopic tumor

experiments, 8–10 week old mice were employed. Both male and female mice were used, but animals were sex- and age-matched within each experiment. Mice were administered intra-pancreatic injections of FC1242 tumor cells derived from pancreata of KPC mice (10^5 cells in Matrigel; BD Biosciences, San Jose, CA) and sacrificed at 3 weeks. We have previously reported the development of the FC1242 cell line[9]. Cells were tested negative for Mycoplasma within the past 2 months. In select experiments, mice were treated with Gemcitabine i.p. (1.2 mg twice weekly; MedChemExpress, Monmouth Junction, NJ). In other experiments, animals received a single intratumoral injection of recombinant murine C3a (40μg/kg; R&D, Minneapolis, MN) on day 14 after orthotopic tumor injections. Mice with pancreatic tumors were monitored regularly for distention of the abdomen, reduced feeding, weight loss, dehydration, hunched posture, or poor grooming habits. On detection of signs or symptoms of distress or when tumor size was estimated by palpation to exceed 15% of the normal body weight, mice were euthanized. Pancreatitis was induced using a regimen of 7 hourly intraperitoneal injections of caerulein (50μg/kg; Sigma-Aldrich, St. Louis, MO) for 3 consecutive days before sacrifice 12 hours later. Serum amylase activity levels in murine serum were measured using the colorimetric mouse amylase assay kit (ab102523, Abcam, Cambridge, MA) according to manufacturer protocols. KPC tumor cell proliferation *in vitro* was assessed using the XTT assay (Sigma-Aldrich). Recombinant mC3a (5nM; R&D) was added to select wells.

Antifungal treatment and fungal transfer experiments

To ablate the mycobiome in mice, animals were administered Amphotericin B (1mg/ml; MP Biomedicals, Santa Ana, CA) by oral gavage daily for five consecutive days in addition to adding Amphotericin B (0.5μg/ml) to mouse drinking water for the duration of the experiment[10]. Controls were gavaged with PBS. Orthotopic PDA tumor cells were administered or pancreatitis was initiated 3 weeks after commencing treatment with Amphotericin B. Alternatively, mice were treated with Fluconazole (0.5mg/ml; MP Biomedicals) for 3 weeks prior to tumor implantation using the same regimen[11]. For species-specific repopulation experiments, *M. globosa* (MYA-4612, 1×10^8 CFU/ml), *S. cerevisiae* (7752, 1×10^8 CFU/ml), *C. tropicalis* (MYA-3404, 1×10^8 CFU/ml; all ATCC Manassas, VA), *Candida sp.* (clinical isolate; 1×10^8 CFU/ml) or *Aspergillus sp.* (clinical isolate; 1×10^6 CFU/ml) were used to orally gavage mice following fungal ablation with Amphotericin B. Recipient mice were administered orthotopic PDA cells 7 days after repopulation. To assess fungal translocation to the pancreas, 10^8 CFU of GFP-labeled *Saccharomyces cerevisiae* (ATCC MYA-2011) were introduced via oral gavage, and pancreatic samples were examined at 30 minutes by flow cytometry. All experiments were approved and in compliance with the New York University School of Medicine Institutional Animal Care and Use Committee (IACUC).

C3aR Knockdown

Lentiviral transfer plasmids against C3aR SHCLNG-NM_009779 (TRCN0000027362; CCAGAAAGCAATTCTACTGAT and TRCN0000027385; CCCGTATTTGTATACCGTGAT) were transformed into Stbl3 bacteria. Plasmids were purified using MaxiPrep Kit (Qiagen, Germantown, MD) and DNA concentration was evaluated by Nanodrop (Thermo Fisher Scientific, Waltham, MA). The transfer plasmids

were co-transfected into HEK293FT cells with packaging plasmids PLP1, PLP2, and VSVG. To evaluate lentivirus concentration, titration of the ability of virus to induce puromycin resistant colonies was performed in HEK293FT cell line. Next, KPC tumor cells were transduced for 48 hr followed by selection with puromycin (2 μg/ul) for 10 days. Efficacy of C3aR knockdown was confirmed by qPCR.

qPCR

Real-time qPCR was performed in duplicate for each sample using the BioRad Real-Time PCR System (BioRad). Each reaction mixture contained 10 μl of SYBR Green Master Mix (Applied Biosystems), 0.5 μl of forward and reverse primers (Invitrogen) and 3 μl of cDNA (corresponding to 50 ng of RNA). The qPCR conditions were: 50°C for 2 minutes, 95°C for 10 minutes, followed by 40 cycles at 95°C for 15 seconds, and 60°C for 1 minute. Amplification of specific transcripts was confirmed by melting curve profiles generated at the end of the PCR program. Expression levels of target genes were normalized to the expression of GAPDH (internal control) and calculated based on the comparative cycle threshold (CT) method ($2^{-\Delta\Delta Ct}$). The *C3aR* primer sequences used in the study were F-TAACCAGATGAGCACCACCA, R- TGTGAATGTTGTGTGCATTG.

Histology, Immunohistochemistry, and Microscopy

For histological analysis, pancreatic specimens were fixed with 10% buffered formalin, dehydrated in ethanol, embedded with paraffin, and stained with H&E or Gomori Trichrome. The percentage of preserved acinar area and fibrosis were calculated, as previously described[1]. The fraction and number of ducts containing all grades of PanIN lesions were measured by examining 10 H&E-stained high-power fields (HPFs; 40X) per slide. PanINs were graded according to established criteria[12]: In PanIN I ducts, the normal cuboidal pancreatic epithelial cells transition to columnar architecture and can gain polyploid morphology. PanIN II lesions are associated with loss of polarity. PanIN III lesions, or in-situ carcinoma, show cribriforming, budding off of cells, and luminal necrosis with marked cytological abnormalities, without invasion beyond the basement membrane. Characteristics of control KC mice were previously detailed[13]. Pancreatic edema was calculated by measuring intra-lobular white space on H&E sections. Immunohistochemistry was performed using antibodies directed against CD45 (30-F11, BD Biosciences), C3a (JF10–30, Novus, Centennial, CO), and DAPI (#H-1200; Vector Labs, Burlingame, CA). For paraffin-embedded slides, samples were dewaxed in ethanol followed by antigen retrieval with 0.01 M Sodium Citrate with 0.05 % Tween.

Fluorescence In Situ Hybridization (FISH)

The D223 28S rRNA gene probe labeled with the 5'Cy3 fluorophore (extinction wavelength, 555 nm; emission wavelength, 570 nm; Molecular Probes, Eugene, OR) was used to detect the fungal colonization within human and mouse pancreatic tissues by FISH. Fluorescence microscopic analysis was conducted with Nikon Eclipse 90i confocal microscope (Nikon, Melville, NY) using a Cy3 labeled-probe at 350 pmol/ml as we described[1].

Human sample collection and TCGA data

Human fecal samples and pancreatic tissue specimens were sterilely collected from healthy volunteers and patients undergoing surgery for either PDA or benign disease (pancreatic endocrine tumors) at NYU Langone Medical Center. Donors were deidentified. Samples were stored at −80°C until analysis. Patients on antibiotic or antifungal treatment within the past 3 months were excluded. Human specimens were collected in compliance with the policies and approval of NYU School of Medicine's Institutional Review Board and conducted in accordance with the Declaration of Helsinki, the Belmont Report, and U.S. Common Rule. Data on gene expression in human tissues was derived from TCGA (https://portal.gdc.cancer.gov/). Survival was measured according to the Kaplan-Meier method and analyzed by log rank.

Fungal DNA extraction and sequencing

Pancreatic tissue samples were suspended in 500 μL sterile PBS and pretreated by vortexing and sonication followed by overnight treatment with Proteinase K (2.5 μg/mL; Thermo Fisher) at 55°C. Total microbial genomic DNA was purified from tissue and fecal samples using the MoBio Power kit as per the manufacturer's instructions (MoBio Laboratories, Carlsbad, CA). DNA was quantified for concentration and purity using the NanoDrop 2000 spectrophotometer (Thermo Fisher) and stored at −20°C. For high throughput ITS library preparation and sequencing, the ITS1 region of the 18S rRNA gene was amplified from the genomic DNA of mice and human fecal and pancreatic tissue samples according to the modified Illumina metagenomics protocol (Part # 15044223 Rev. B). The purified DNA was quantified fluorometrically by Quant-iT PicoGreen assay (Molecular Probes, Eugene, OR) in a SpectraMax M5 microplate reader (Molecular Devices, Sunnyvale, CA), and the concentration was adjusted to 10 ng/μL for all sequencing assays. PCR was initially performed using the primer set ITS1F (5'-CTTGGTCATTTAGAGGAAGTAA −3') and ITS2 (5'-GCTGCGTTCTTCATCGATGC-3')[14]; each with overhang adapter sequences (IDT, Coralville, IA) using 2x Kapa HiFi Hotstart ReadyMix DNA polymerase (KapaBiosystems, Wilmington, MA). Samples were amplified in duplicates and purified using AMPure XP beads. Amplification was performed at 95°C (5 min), with 25 cycles of 95°C (1 min), 53°C (45 sec), 72°C (1 min), and final extension of 72°C (10 min). Dual indices from Illumina Nextera XT index kits (Illumina, San Diego, CA) were added to target amplicons in a second PCR using the 2x Kapa HiFi Hotstart ReadyMix DNA polymerase. PCR conditions were 95°C (5 min), with 10 cycles of 95°C (1 min), 53°C (45 sec), 72°C (1 min), and final extension of 72°C (10 min). After each PCR cycle, AMPure XP beads purified libraries were checked for purity by Nanodrop, quantified by PicoGreen assay, and size confirmed on agarose gels. Negative controls were included in all sequencing runs. Equimolar amounts of the generated libraries were combined and quantified fluorometrically. The pooled amplicon library was denatured, diluted, and sequenced on an Illumina MiSeq platform using MiSeq Reagent Kit v3 (600 cycles) following the 2×300-bp paired-end sequencing protocol.

Bioinformatics and Statistical analyses

The Illumina-generated fungal ITS sequence data was processed using QIIME (v1.9.1) and the reads demultiplexed, quality filtered, and clustered into operational taxonomic units (OTUs) using default parameters[15]. To maintain consistency, Read1 was used for the analyses as described[14]. Prior to demultiplexing, the 5' primers of a total 16,647,630 R1 reads were trimmed using cutadapt (v1.12), and sequences shorter than 100 bases or sequences including Ns were discarded. The reads were filtered by quality at 20 using multiple_split_libraries_fastq.py (q = 19 and defaults were used for other parameters). The 1,989,618 quality reads (Mean 8575; n=166) were then processed with QIIME. Chimeric sequences were removed using VSEARCH (v2.4.3) with UNITE UCHIME reference dataset (v7.2). OTUs were picked with open reference OTUs picking method with default parameters against UNITE reference database (v7.2) to assign taxonomy using pick_open_reference_otus.py[16]. OTUs (126862) corresponding to 1,856,993 reads (~93.57%) that failed to align to fungi were excluded from the downstream analyses. OTUs which were unidentified in UNITE database were blasted to NCBI, and the taxonomy information of best hit (similarity/coverage ≥97%) for each OTU was re-assigned. A total of 127,646 sequence reads were clustered into 1899 OTUs (86,640 reads) for longitudinal mouse fecal samples; 390 OTUs (25,021 reads) for mouse tissue samples; 2980 OTUs (15,349 reads) for human fecal samples; and 311 OTUs (636 reads) for human tissue samples. Sequence data were analyzed at various levels of phylogenetic affiliations. Low abundance OTUs in <2 samples and samples identified as outliers were removed. The significant distinctions in mycobiotal compositions between cohorts and within samples over time were computed by Mann-Whitney U test. Alpha diversity and beta-diversity were computed and plotted in Phyloseq. Principal coordinate analyses (PCoA) were performed on Bray-Curtis dissimilarity indices, and one-way permutational multivariate analysis of variance (PERMANOVA) was used to test for significant differences between cohorts (Adonis, R package Vegan v2.4.5). p values <0.05 were considered significant.

Quality Control

For quality control, we employed best practices for microbiome- and mycobiome-based studies as we described[1]. All the samples were collected using sterile technique. All PCR reagents were regularly checked for environmental contaminants using ITS universal primers. All qPCR reactions had appropriate controls (without template) to exclude DNA contaminants. To control for the quality of our sequencing, we used both predetermined mock communities (e.g. *C. tropicalis*) and "negative" (reagent-only) controls to check background contamination and sequencing error rate. We included these controls in each sequencing run. We further confirmed the quality of our sequencing by including community controls composed of predetermined ratios of DNA from a mixture of 3 distinct fungal species.

Extended Data

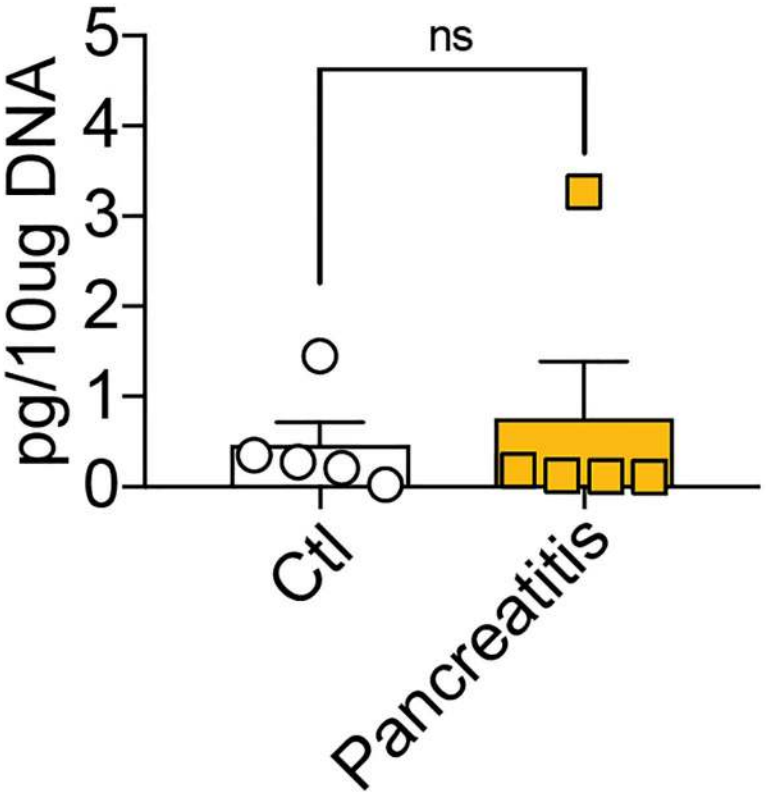

Extended Data Fig. 1. Fungal infiltration of the pancreas in benign disease.

Fungal DNA content was tested using qPCR in pancreata from control mice (n=5) and mice induced to develop caerulein pancreatitis (n=5). NS, non significant. Data are mean ± s.e.m. Two-tailed Student's *t*-test.

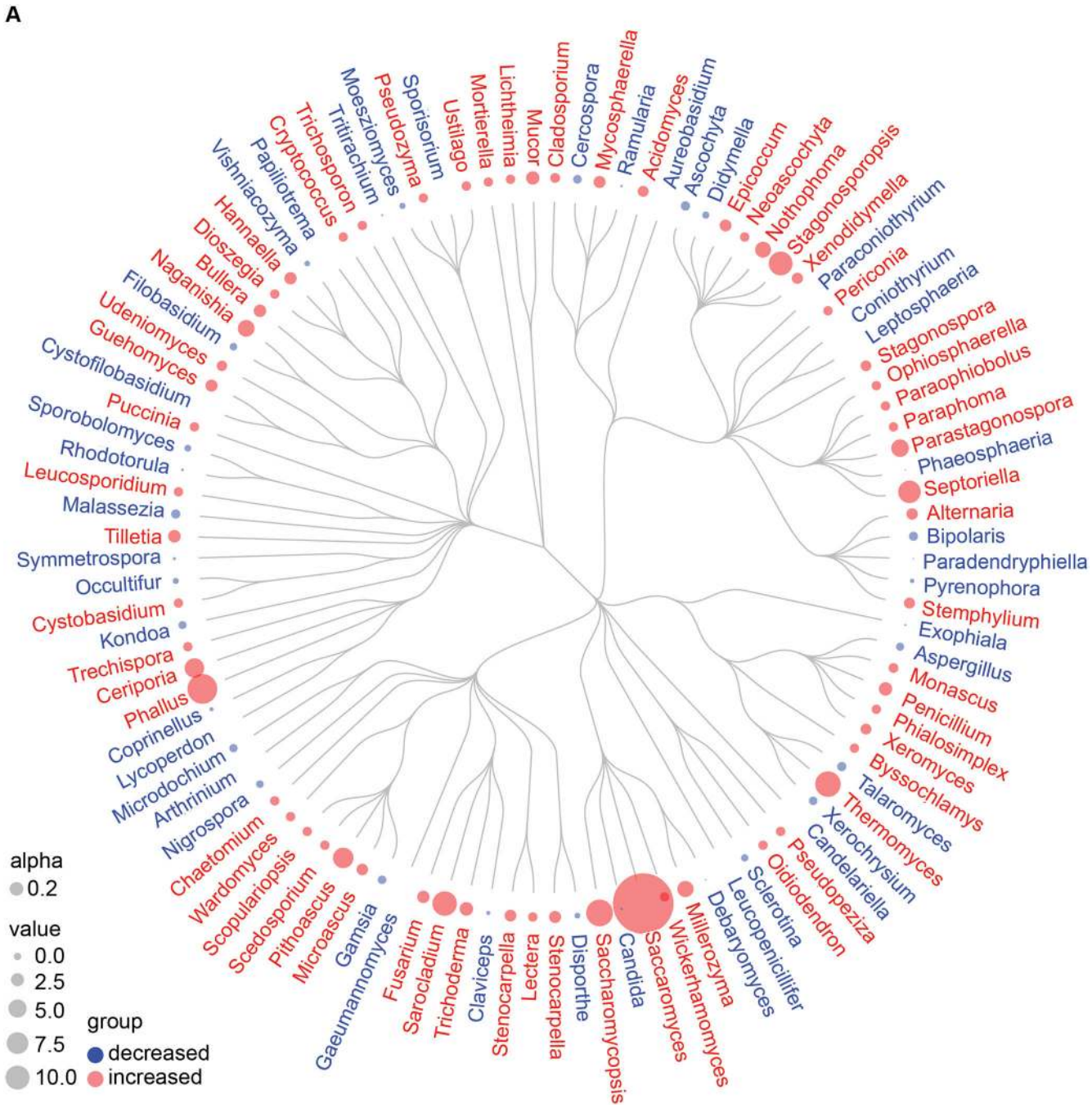

Extended Data Fig. 2. Gut mycobial dysbiosis in murine PDA.

Hierarchical tree cladogram depicting changes in taxonomic composition of mycobiota assigned to genus level in the gut of 30 week old WT (n=12) and KC (n=14) mice based on average percent relative abundance as determined by 18S ITS sequencing.

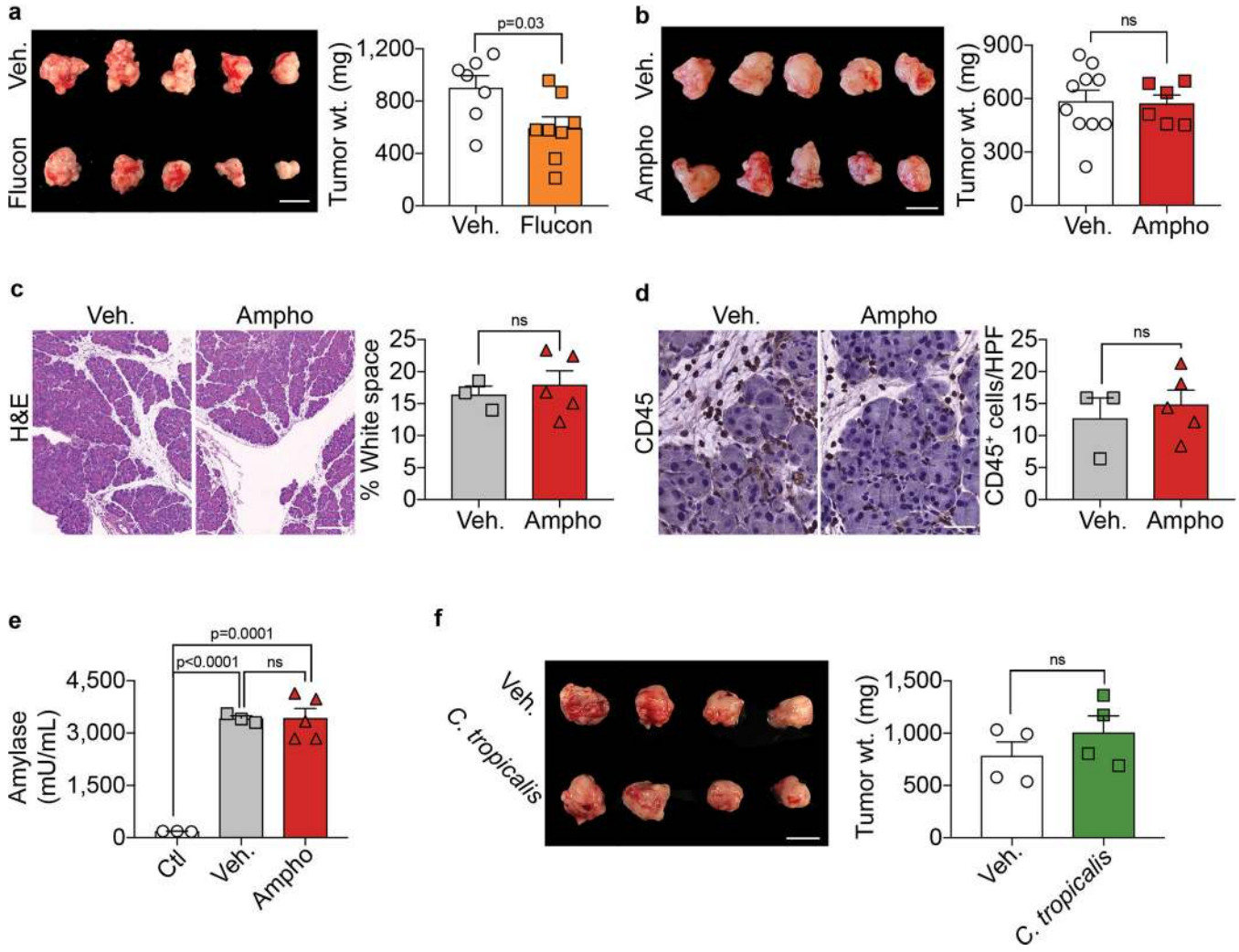

Extended Data Fig. 3. Efficacy of anti-fungal treatments in pancreatic disease.

(A) Orthotopic PDA bearing WT mice were treated with vehicle (n=7) or Fluconazole (n=8) and sacrificed 3 weeks later. Tumors were harvested and weighed. Data are representative of experiments performed twice (scale bar =1cm). Data are mean ± s.e.m. Two-tailed Student's *t*-test. **(B)** Germ-free WT mice were treated with Amphotericin B (n=6) or vehicle (n=10) and administered orthotopic KPC tumor. Mice were sacrificed 3 weeks later and tumors were harvested and weighed (scale bar = 1cm). Data are mean ± s.e.m. Two-tailed Student's *t*-test. **(C-E)** WT mice induced to develop caerulein pancreatitis were serially treated with Amphotericin B (n=5) or vehicle (n=3). (C) Representative H&E sections of pancreata are shown, and pancreatic edema was quantified by measuring the percentage of white space area (scale bar = 100μm). (D) $CD45^+$ inflammatory cell infiltration was determined by IHC (scale bar = 20μm). (E) Serum amylase was measured (n=5 Amphotericin B, n=3 vehicle and n=3 mock-treated animals). Data are mean ± s.e.m. Two-tailed Student's *t*-test. **(F)** Amphotericin B-treated WT mice were repopulated with *C. tropicalis* (n=4) or vehicle (n=4) and sacrificed 3 weeks later. Tumors were harvested and weighed (scale bar =1cm). NS, non significant. Data are mean ± s.e.m. Two-tailed Student's *t*-test.

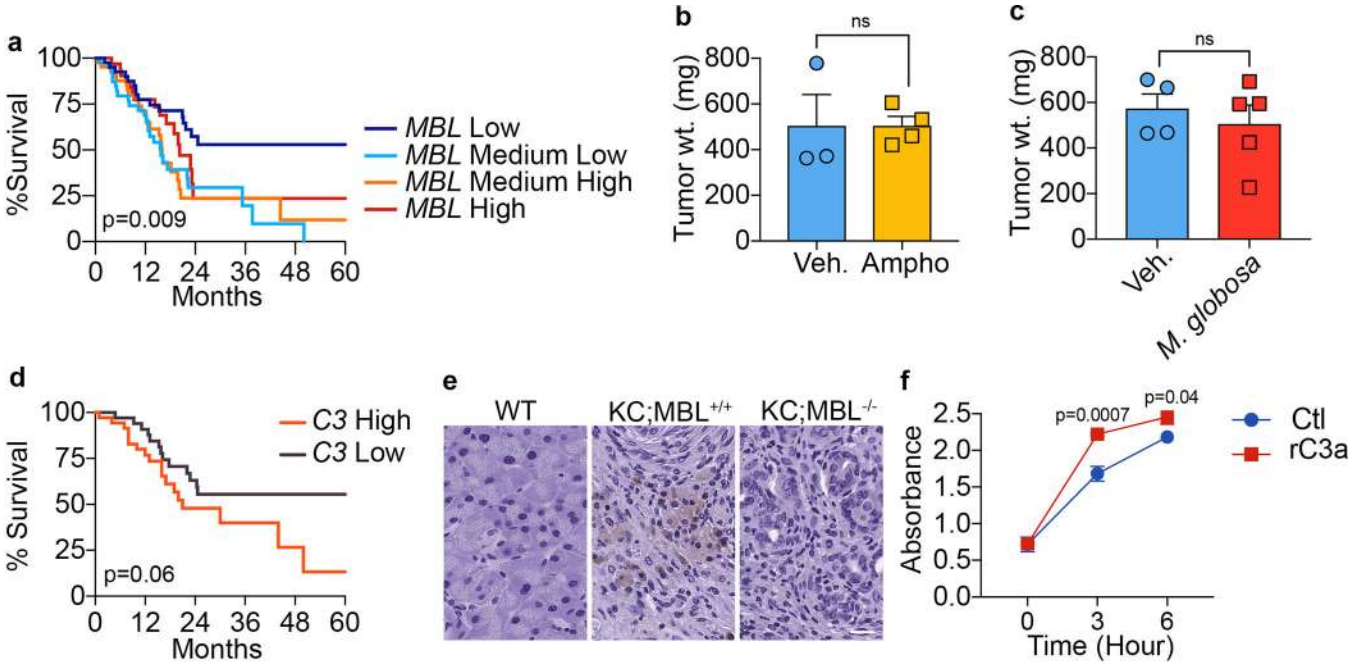

Extended Data Fig. 4. Fungal dysbiosis drives PDA progression via the lectin pathway.

(A) Kaplan-Meier survival curve of human PDA patients stratified by high (n=16), medium high (n=24), medium low (n=26) and low (n=17) *MBL* expression based on TCGA data. Two-tailed log-rank test. **(B)** Vehicle (n=3) and Amphotericin B-treated (n=4) MBL-null mice were administered orthotopic KPC tumors and sacrificed 3 weeks later. Tumors were harvested and weighed. Data are representative of 3 separate experiments. NS, non significant. Data are mean ± s.e.m. Two-tailed Student's *t*-test. **(C)** Amphotericin B-treated MBL-null mice were repopulated with *M. globosa* (n=5) or sham (n=4) repopulated and sacrificed 3 weeks later. Tumors were harvested and weighed. Data are representative of experiments repeated twice. NS, non significant. Data are mean ± s.e.m. Two-tailed Student's *t*-test. **(D)** Kaplan-Meier survival curve of human PDA patients stratified by high (n=18) versus low (n=15) *C3* expression based on TCGA data based on TCGA data. Two-tailed log-rank test. **(E)** Pancreata from 3 month-old WT, KC, and KC;MBL$^{-/-}$ were stained using an mAb against C3a. Representative images from two experiments are shown (scale bar = 20μm). **(F)** KPC tumor cells were seeded in 96-well plates with vehicle or recombinant murine C3a (n=5 per group for each time point). Cellular proliferation was measured at serial time points using the XTT assay. Data are mean ± s.e.m. Two-tailed Student's *t*-test. Data are representative of experiments repeated three times.

Supplementary Material

Refer to Web version on PubMed Central for supplementary material.

Acknowledgements

We acknowledge the use of the Experimental Pathology and Microscopy core facilities at NYU School of Medicine. These shared resources are partially supported by the Cancer Center Support Grant, P30CA016087, at the Laura and Isaac Perlmutter Cancer Center.

Grant Support: This work was supported by NIH grants CA168611 (GM), CA206105 (GM, DS), CA215471 (GM), CA19311 (GM), DK106025 (GM), DE025992 (DS, XL), UL1TR001445 (JIK), Department of Defense grant CA170450 (GM) and Deutsche Forschungsgemeinschaft Grant AY 126/1-1 (BA).

References

1. Pushalkar S et al. The Pancreatic Cancer Microbiome Promotes Oncogenesis by Induction of Innate and Adaptive Immune Suppression. Cancer Discov 8, 403–416, doi: 10.1158/2159-8290.CD-17-1134 (2018). [PubMed: 29567829]
2. Hingorani SR et al. Preinvasive and invasive ductal pancreatic cancer and its early detection in the mouse. Cancer cell 4, 437–450 (2003). [PubMed: 14706336]
3. Hingorani SR et al. Trp53R172H and KrasG12D cooperate to promote chromosomal instability and widely metastatic pancreatic ductal adenocarcinoma in mice. Cancer Cell 7, 469–483, doi:10.1016/j.ccr.2005.04.023 (2005). [PubMed: 15894267]
4. van Asbeck EC, Hoepelman AI, Scharringa J, Herpers BL & Verhoef J Mannose binding lectin plays a crucial role in innate immunity against yeast by enhanced complement activation and enhanced uptake of polymorphonuclear cells. BMC Microbiol 8, 229, doi: 10.1186/1471-2180-8-229 (2008). [PubMed: 19094203]
5. Ishikawa T et al. Identification of distinct ligands for the C-type lectin receptors Mincle and Dectin-2 in the pathogenic fungus Malassezia. Cell Host Microbe 13, 477–488, doi:10.1016/j.chom.2013.03.008 (2013). [PubMed: 23601109]
6. Afshar-Kharghan V The role of the complement system in cancer. The Journal of clinical investigation 127, 780–789, doi:10.1172/JCI90962 (2017). [PubMed: 28248200]
7. Cho MS et al. Autocrine effects of tumor-derived complement. Cell Rep 6, 1085–1095, doi:10.1016/j.celrep.2014.02.014 (2014). [PubMed: 24613353]
8. Sam QH, Chang MW & Chai LY The Fungal Mycobiome and Its Interaction with Gut Bacteria in the Host. Int J Mol Sci 18, doi:10.3390/ijms18020330 (2017).
9. Zambirinis CP et al. TLR9 ligation in pancreatic stellate cells promotes tumorigenesis. J Exp Med 212, 2077–2094, doi:10.1084/jem.20142162 (2015). [PubMed: 26481685]
10. Reikvam DH et al. Depletion of murine intestinal microbiota: effects on gut mucosa and epithelial gene expression. PloS one 6, e17996, doi:10.1371/journal.pone.0017996 (2011). [PubMed: 21445311]
11. Skalski JH et al. Expansion of commensal fungus Wallemia mellicola in the gastrointestinal mycobiota enhances the severity of allergic airway disease in mice. PLoS Pathog 14, e1007260, doi:10.1371/journal.ppat.1007260 (2018). [PubMed: 30235351]
12. Hruban RH et al. Pancreatic intraepithelial neoplasia: a new nomenclature and classification system for pancreatic duct lesions. Am J Surg Pathol 25, 579–586 (2001). [PubMed: 11342768]
13. Seifert L et al. The necrosome promotes pancreatic oncogenesis via CXCL1 and Mincle-induced immune suppression. Nature 532, 245–249, doi:10.1038/nature17403 (2016). [PubMed: 27049944]
14. Walters W et al. Improved Bacterial 16S rRNA Gene (V4 and V4–5) and Fungal Internal Transcribed Spacer Marker Gene Primers for Microbial Community Surveys. mSystems 1, doi: 10.1128/mSystems.00009-15 (2016).
15. Navas-Molina JA et al. Advancing our understanding of the human microbiome using QIIME. Methods Enzymol 531, 371–444, doi:10.1016/B978-0-12-407863-5.00019-8 (2013). [PubMed: 24060131]
16. Caporaso JG et al. QIIME allows analysis of high-throughput community sequencing data. Nat Methods 7, 335–336, doi:10.1038/nmeth.f.303 (2010). [PubMed: 20383131]

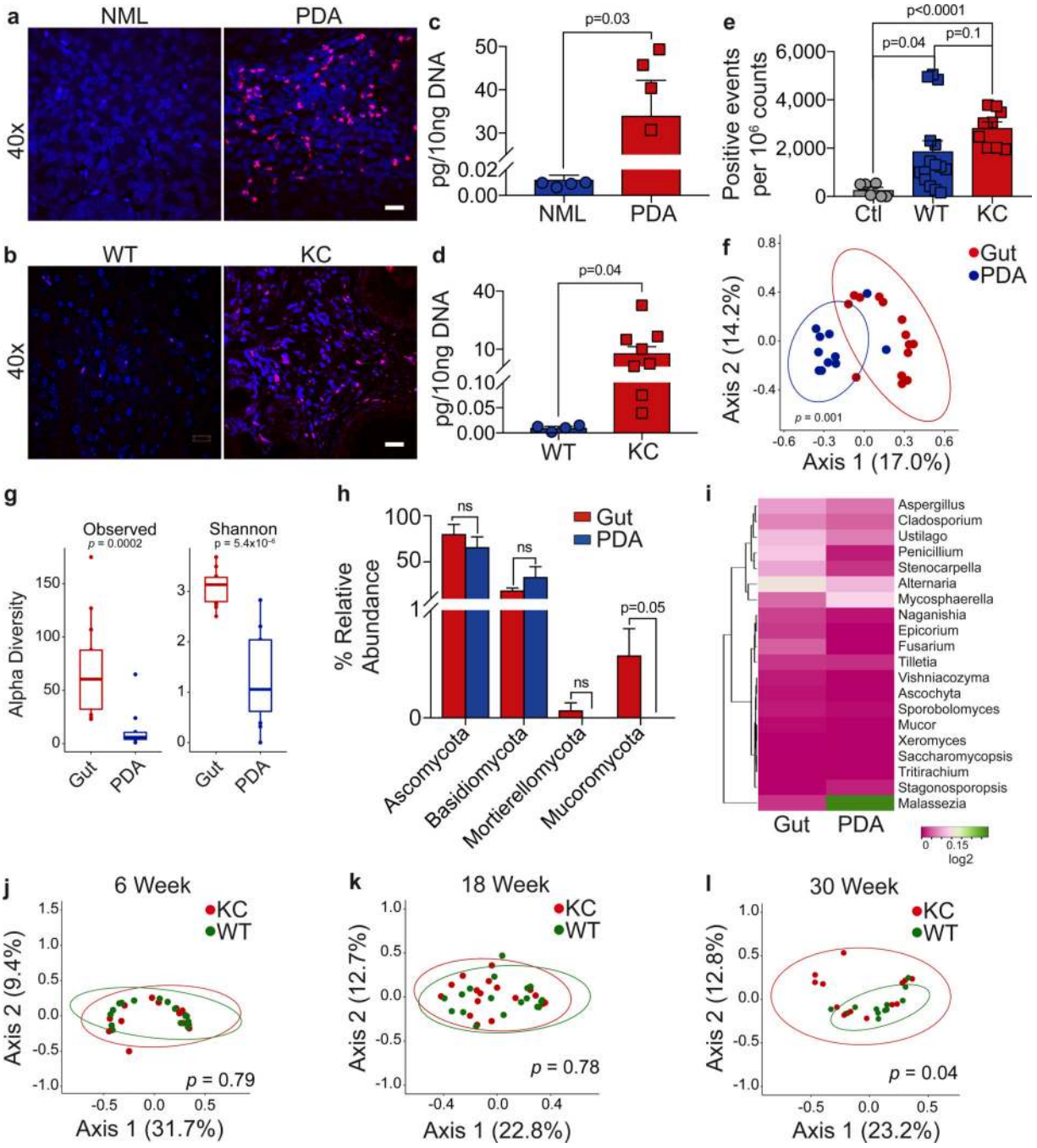

Fig. 1. PDA is characterized by a distinctive intra-tumoral and gut mycobiome.

(A) The abundance of intra-pancreatic fungi was compared in healthy individuals (NML) and age/gender/BMI matched PDA patients by FISH (n=3/group). Representative images are shown (scale bar = 20μm). **(B)** The abundance of intra-pancreatic fungi was compared in 3-month-old littermate WT and KC mice by FISH. Representative images are shown (n=3/group; scale bar = 20μm). **(C)** Fungal DNA content was compared in pancreata of healthy individuals and age/gender/BMI matched PDA patients using qPCR. Data are mean ± s.e.m. Two-tailed Student's *t*-test. **(D)** Fungal DNA content was compared in pancreata of 3-

month-old WT and KC mice using qPCR. Data are mean ± s.e.m. Two-tailed Student's *t*-test. **(E)** WT (n=15) and KC (n=9) mice were administered GFP-labeled *S. cerevisiae* via oral gavage. Pancreata were harvested at 30 minutes and the number of GFP^+ foci was determined by flow cytometry in comparison to mock-treated animals (n=6). This experiment was repeated twice. Data are mean ± s.e.m. Two-tailed Student's *t*-test. **(F-I)** The gut (n=14 biologically independent samples) and intrapancreatic (n=11 biologically independent samples) mycobiomes in 30 week-old KC mice were analyzed by 18S ITS sequencing. (F) PCoA plots based on Bray-Curtis dissimilarity matrix. Each symbol represents a sample from gut (red) or pancreas (blue). Clusters were determined by pairwise PERMANOVA. X- and Y-axes indicate percent variation and the ellipses indicate 95% confidence interval (CI). (G) The gut and intra-pancreatic mycobiomes in 30 week-old KC mice were analyzed for alpha-diversity measures including Observed OTUs and Shannon indices. Two-sided Wilcoxon rank-sum test. Box plots show median, 25th and 75th percentiles, and whiskers extending to 1.5 interquartile ranges. (H) Taxonomic composition of mycobiota assigned to the phylum level based on average percent relative abundance. NS, non significant. Data are mean ± s.e.m. Two-tailed Student's *t*-test. (I) Heatmap showing log2-transformed relative abundancies of top 20 fungal genera in gut and pancreata. **(J-L)** PCoA plots of fungal communities in feces of (J) 6-week, (K) 18-week, and (L) 30-week old WT and KC mice based on Bray-Curtis dissimilarity matrix. Clusters were determined by pairwise PERMANOVA. X- and Y-axes indicate percent variation and the ellipses indicate 95% CI.

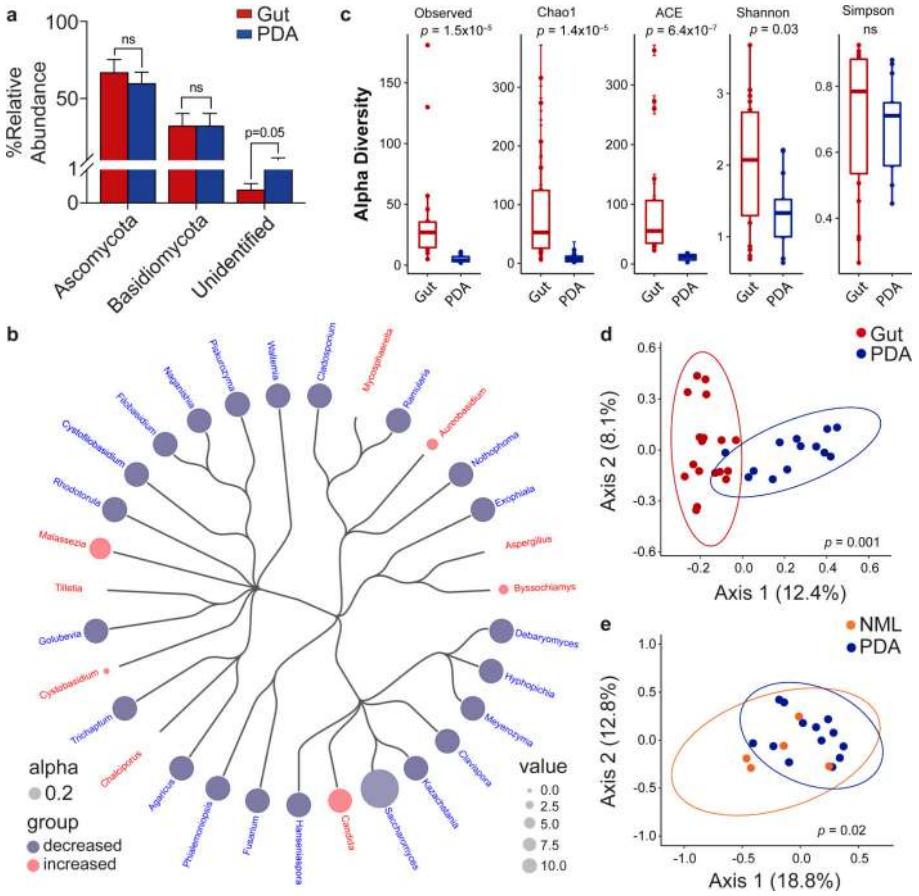

Fig. 2. Human PDA is associated with a distinct mycobiome.

(A-D) Gut (n=18) and Tumor (n=13) of specimens from PDA patients were analyzed by 18S ITS sequencing. (A) Taxonomic composition of mycobiota assigned to the phylum level based on average percent relative abundance. NS, non significant. Data are mean ± s.e.m. Two-tailed Student's *t*-test. (B) Hierarchical tree cladogram depicting differences in taxonomic composition of mycobiota assigned to genus level in gut and tumor based on average percent relative abundance. (C) The gut and tumor mycobiome of PDA patients were tested for alpha-diversity measures including Observed OTUs, ACE, Chao1, Shannon, and Simpson indices. Two-sided Wilcoxon rank-sum test. Box plots show median, 25th and 75th percentiles, and whiskers extending to maximum and minimum data points. (D) PCoA plots of gut (n=18) and intra-tumoral (n=13) fungal communities in PDA patients based on Bray-Curtis dissimilarity matrix. (E) PCoA plots of fungal communities in pancreata of PDA patients (n=13) and healthy individuals (n=5) based on Bray-Curtis dissimilarity matrix. Analyses were determined by pairwise PERMANOVA. X- and Y-axes indicate percent variation and the ellipses indicate 95% CI.

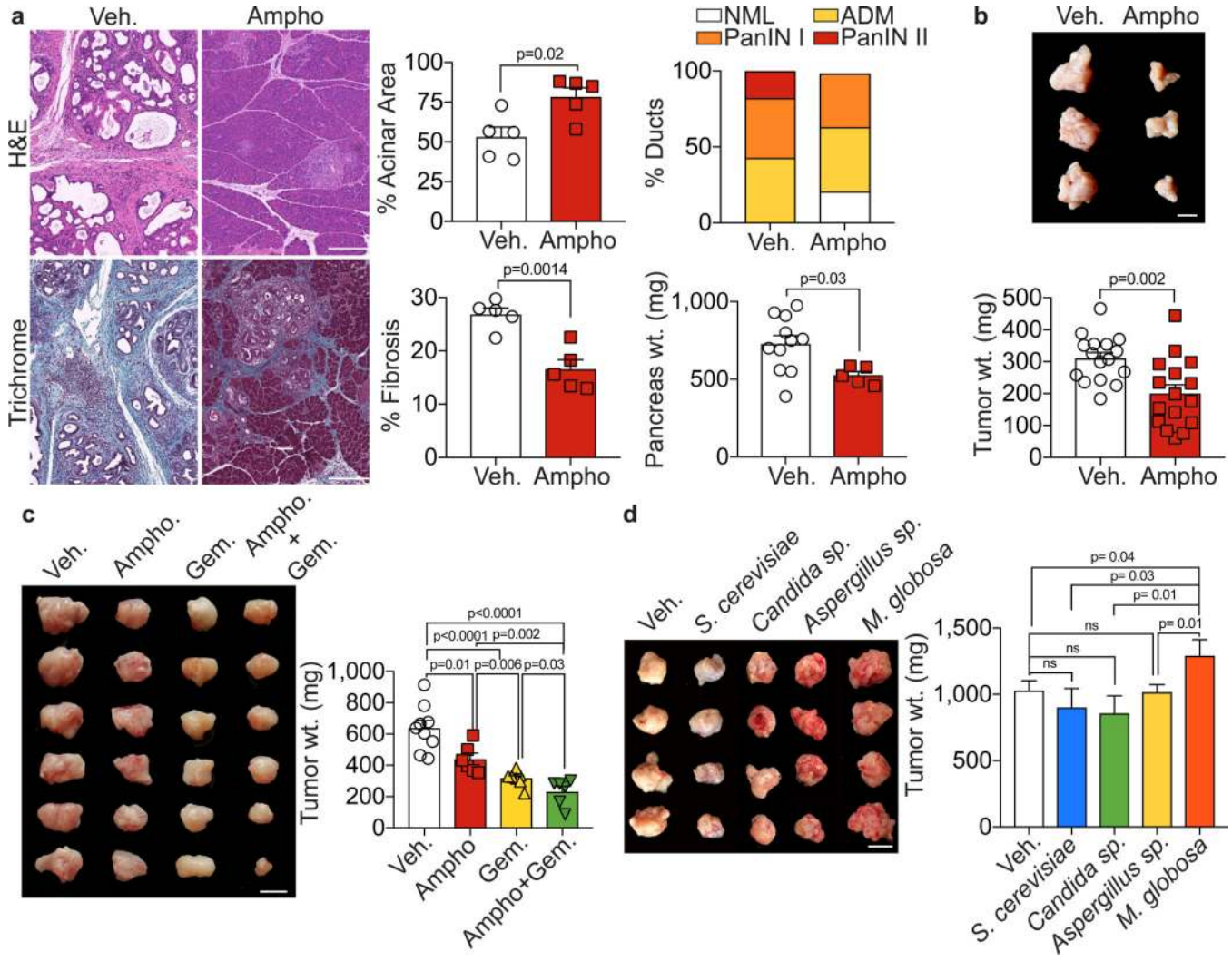

Fig. 3. Fungal dysbiosis promotes pancreatic oncogenesis.

(A) Amphotericin B and Vehicle-treated KC mice were sacrificed at 3 months of life. Pancreatic weights (n=5 and 11, respectively) were recorded. Representative H&E- and trichrome-stained sections are shown. The percentage of preserved acinar area, and the fraction of normal ducts, acinoductal metaplasia, and graded PanIN lesions were determined based on H&E staining (scale bar = 200μm). The fraction of fibrotic area per pancreas was calculated based on trichrome staining (scale bar = 200μm). Data are mean ± s.e.m. Two-tailed Student's *t*-test. **(B)** Orthotopic PDA bearing WT mice were treated with vehicle or Amphotericin B (n=16 per group, data pooled from three independent experiments) and sacrificed 3 weeks later. Tumors were harvested and weighed. Data are representative of experiments repeated more than 5 times (scale bar =1cm). Data are mean ± s.e.m. Two-tailed Student's *t*-test. **(C)** Orthotopic PDA bearing WT mice were treated with vehicle (n=9), Amphotericin B (n=6), Gemcitabine (n=8), or Amphotericin B + Gemcitabine (n=6). Tumor weight was recorded at 3 weeks (scale bar =1cm). Data are mean ± s.e.m. Two-tailed Student's *t*-test. **(D)** Amphotericin B-treated WT mice were repopulated with *M. globosa* (n=8), *S. cerevisiae* (n=9), *Candida sp.* (n=8), or *Aspergillus sp.* (n=10) or vehicle (n=8) and

sacrificed 3 weeks later. Tumors were harvested and weighed. Data are representative of experiments repeated twice (scale bar =1cm). NS, non significant. Data are mean ± s.e.m. Two-tailed Student's *t*-test.

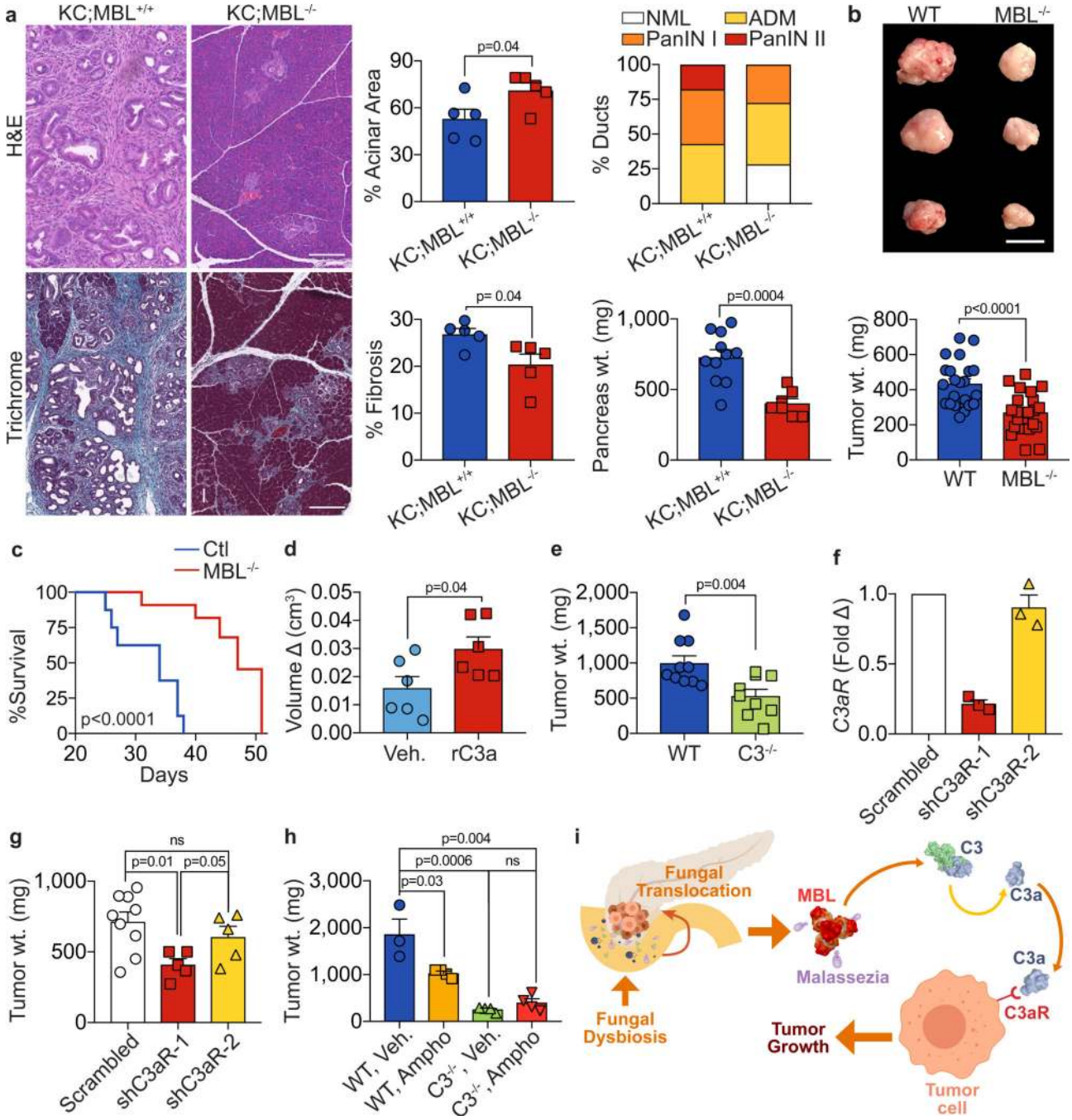

Fig. 4. Fungi promote PDA progression via the MBL – C3 axis.

(A) KC (n=11) and KC;MBL-null (n=7) mice were sacrificed at 3 months of life. Tumors were weighed and stained using H&E (scale bar = 200μm), trichrome (scale bar = 200μm), and analyzed for pancreatic dysplasia and fibrosis. Data for control KC is the same as in Fig. 3. Data are mean ± s.e.m. Two-tailed Student's *t*-test. **(B, C)** WT and MBL-null mice were administered orthotopic KPC tumor and analyzed for (B) tumor growth at 3 weeks (n=22 per arm; data represent mean ± s.e.m, two-tailed Student's *t*-test) and (C) survival (n=8 WT and n=5 MBL-null animals; log-rank test). Data are representative of experiments repeated more

than 5 times. **(D)** $MBL^{-/-}$ hosts were administered orthotopic KPC tumors and received intratumoral injections of recombinant C3a (n=6) or vehicle (n=6) on day 14 via laparotomy, and tumor volumes were measured. Tumors were harvested on day 21, and change in tumor volume since injection was calculated. This experiment was repeated twice. Data are mean ± s.e.m. Two-tailed Student's *t*-test. **(E)** WT (n=10) and $C3^{-/-}$ (n=9) mice were administered orthotopic KPC tumor and analyzed for tumor growth at 3 weeks. Data are representative of experiments repeated 3 times. Data are mean ± s.e.m. Two-tailed Student's *t*-test. **(F, G)** WT mice were orthotopically implanted with KPC tumors cells treated with either shRNA directed against C3aR or control scrambled shRNA. Separate shRNA vectors were used. (F) The efficacy of C3aR knockdown was measured by qPCR (n=3 per group). Data are mean ± s.e.m. Two-tailed Student's *t*-test. (G) Quantitative analysis of day 21 tumor weights is shown (n=9 for scrambled and n=5 for shC3aR1 and shC3aR2). Data are mean ± s.e.m. Two-tailed Student's *t*-test. **(H)** Vehicle (n=3–4) and Amphotericin B-treated (n=4) WT and $C3^{-/-}$ mice were administered orthotopic KPC tumors and sacrificed 3 weeks later. Tumors were harvested and weighed. Data are representative of experiments repeated twice. Data are mean ± s.e.m. Two-tailed Student's *t*-test. **(I)** Schematic depicting mycobiome-MBL axis in pancreatic oncogenesis.